EXPERIMENTAL INVESTIGATION ON BRINE RECIRCULATION PUMPS IN A DESALINATION PLANT

L. Carassale, A. Stocchino, F. Percivale, M. Colombini
Dept. of Civil Environmental and Architectural Engineering, University of Genova, Genova, Italy

S. Rebagliati, M. Bucello
Fisia Italimpianti S.p.A., Genova, Italy

ABSTRACT

An extensive field campaign measurements performed on a unit of a Multi-Stage Flash (MSF) desalination plant is reported. In particular, the attention is focused on a single Brine Recirculation Pump (BRP) instrumented by accelerometers, miniature pressure sensors, strain gauges and position probes in order to investigate its vibrational response generated by pressure field oscillations, probably due to cavitation and/or suction recirculation. Data were collected either during the startup of the plant and at different working conditions, in terms of head and flow. The analysis of the data reveals a fairly complicated spectral behavior both in the vibrations and pressure fields. In particular, as the suction pressure decrease, intense and persistent spectral peaks appear generating large-amplitude vibrations.

1. INTRODUCTION

Desalination plants based of the Multi-Stage Flash (MSF) principle produce fresh water via partial distillation of seawater. The byproduct of the process is a high-concentrate seawater at temperature ranging about 40 – 50 °C that is recirculated in the plant by pumps referred to as Brine Recirculation Pumps (BRP). BRPs are the largest pumps in MSF desalination plants, are usually coupled in parallel (two for each distiller) and are vertically mounted in barrels that form their intake wells. Each barrel is fed by a suction line connected to the last stage of the distiller, where the brine is kept close to its vapor pressure by a vacuum system. BRPs deliver the brine through the condenser bundles to the brine heater and back to the first stage of the distiller.

Due to economical reasons, the size of the distillers is constantly increasing as a rate such that almost any new realization is the largest ever built. As a consequence of this trend, unpredicted phenomena frequently become relevant due to the change of scale, causing reliability concerns for plant constructors and managers, as well as the necessity of implementing retrofitting solutions.

BRPs problems are typically related to the limited NPSH available that may produce cavitation and to the necessity of driving the pumps quite far from the best efficiency point due to transient process requirements. These circumstances also exasperate many problems typical of large-size pumps related to local and global unsteady flow oscillations that may produce large amplitude vibrations.

The present paper describes the results of an extensive experimental campaign on a set of BRPs affected by large-amplitude vibration, noise and erosion on the pump surfaces in the neighborhood of the impeller. The pumps are double-suction, single-stage realizations capable of the nominal flow rate Q=14800 m3/h and head H=90m; the impeller speed is 500 rpm, while the motor power is about 5MW.

In particular, one pump was instrumented by accelerometers pressure sensors, strain gauges and position probes, while its suction line was instrumented by pressure sensors, doppler profilometers and sensors for measuring the vapor bubble concentration. In the present paper we concentrate on the vibration and pressure measurements on the BRP.

The data-interpretation stage included, besides the standard spectral analysis of all the relevant working regimes, the study of some nominally-stationary time-windows by means of frequency-domain techniques such as the Spectral Kurtosis (Ottonello & Pagan 1994) for the detection of pure-tone components and the Proper Orthogonal Decomposition (Holmes et al 1996) for the identification of coherent modes in the pressure field as well as in the motion of the pump frame. The two above techniques were jointly adopted to identify the first operation vibration modes of the pump.

In this context, it is worth mentioning the detection of narrow-band spectral contents, identified as pure-tones, visible both in the vibration, as well as in all the pressure measurements. These spectral components, visible only when the suction pressure is below a certain value, shows some peculiar behavior with a marked dependency of their peak frequency on the flow rate, giving rise, also thanks to their nonlinear interactions rotation frequency and the blade-passing frequency, to quite complicate spectral

patterns. The presence of these fluid-induced excitations was particularly relevant since, for some working conditions of the plant, two of them had peak frequency very close the first two natural frequencies of the pump frame producing large-amplitude vibrations.

2. EXPERIMENTAL SETUP

Four accelerometers were installed on the pump casing as shown in Figure 1 in such a way to measure the horizontal vibration of the pump at the level of the upper bell mouth and at the level of the lower flange of the column pipe. All the accelerometers were piezoelectric ones with sensitivity 100 mV/g, 50 g range.

Eighteen pressure sensors were installed on the inner and outer surfaces of the two suction bells (Fig. 1c). The sensor setup was defined of the base of the erosion traces detected during previous inspections.

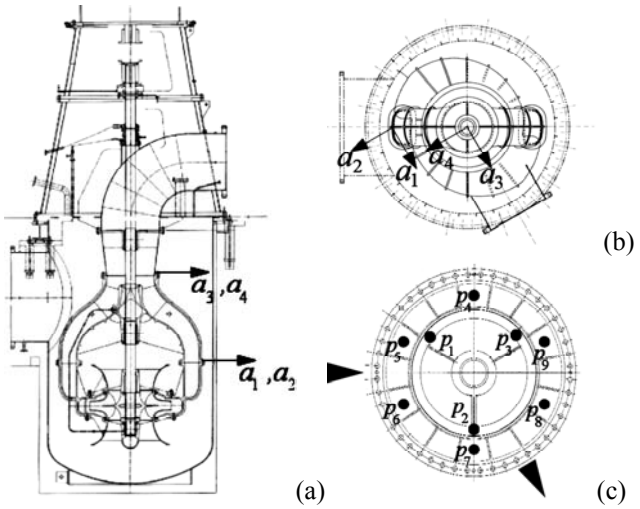

Figure 1: *Experimental setup. Accelerometers* (*a, b*)*, pressure sensors on the upper bell-mouth* (*c,* p_1 - p_3 *inside;* $p_4 - p_9$ *outside*).

Of the nine sensors positioned on each bell mouth, three (p_1-p_3) were placed on their inner surface, while six (p_4-p_9) were installed on their outer surface. The former were installed relatively close to the impeller, at the boundary of the eroded region; the latter were positioned close to the pump body, in a region not interested by evident erosion. The sensors adopted were piezo-resistive ones with working range equal to 20 bar and surviving range up to 60 bar.

Acceleration and pressure signals (as well as all the signal not considered in the present paper) were simultaneously sampled at 1 kHz rate, digitalized by a 16-bit converter and continuously recorded on a computer. Signal pre-filtering was provided in order to prevent measurement and digitalization errors.

3. MEASUREMENTS

Measurements were acquired continuously along a whole startup operation of the plant. The instrumented pump was started receiving brine from the distiller at ambient temperature and atmospheric pressure. Then, the vacuum was produced reaching, in last stage of the distiller, an absolute pressure about 30 mbar, corresponding to an NPSH available at the inlet flange of the pump about 4.5 m. The brine temperature was progressively increased reaching a value about 30°C (Fig. 2a). During this phase, the pump worked at its minimum flow as per manufacturer specifications, while the discharge pressure changed as a mere consequence of the reduction in the suction pressure (Fig. 2b).

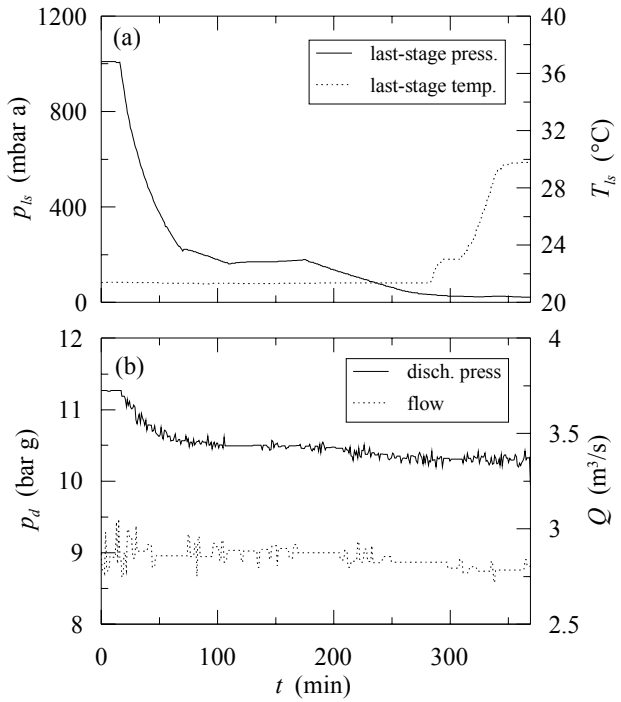

Figure 2: *Main working parameters during startup; last-stage temperature and pressure* (*a*)*, flow and discharge pressure* (*b*).

After the startup, the plant was operated in such a way to span all the relevant flow conditions (actually used operation) by throttling a valve on the discharge line (Fig. 3a). The discharge pressure (Fig. 3a), as well as the last stage pressure and temperature (Fig. 3b) changed according to the pump characteristic curve and to the process requirements.

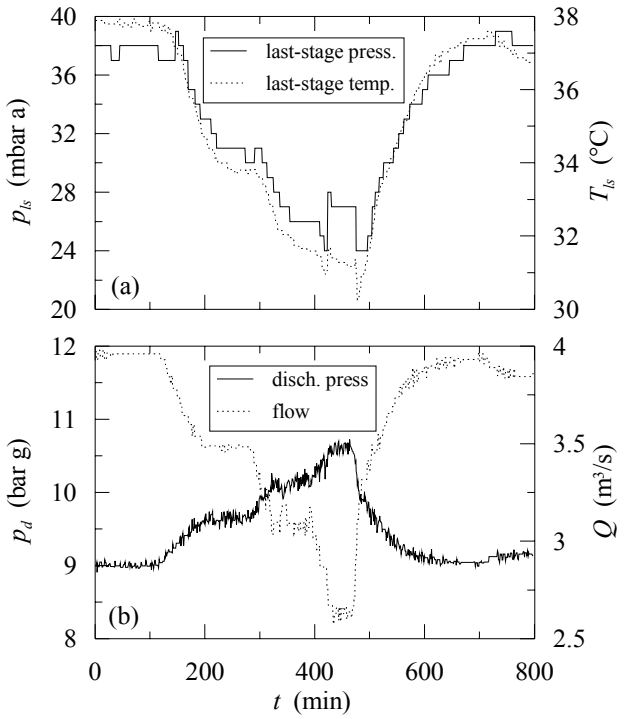

Figure 3: *Main working parameters during plant operation; last-stage temperature and pressure* (*a*)*, flow and discharge pressure* (*b*).

4. DATA ANALYSIS

A preliminary analysis of all the measured signals consisted in the evaluation of the mean and root-mean-square (rms) values in two-minute-long time windows moving along the whole duration of the test. Then, the fluctuating part of the signals (obtained deducing from the measurements the aforementioned mean values) was analyzed by means of the standard spectral analysis. It was noted that the qualitative behavior of both the pressure and acceleration measurements was characterized by the presence of several spectral peaks forming a quite complex pattern changing as a function of the working condition.

In order to explore the nature of such a spectral peaks, the plant was operate in such a way to maintain the pumps in a nominally-stationary condition for a conveniently-long time, allowing the application of the mathematical tools typical of analysis of stationary random processes such as the frequency-domain representation. Besides the classical spectral analysis, two frequency-domain techniques such as the Spectral Kurtosis (SK) (Ottonello & Pagan 1994) and the Proper Orthogonal Decomposition (POD) (e.g. Holmes at al 1996) were applied as well. Their mathematical definition and their properties are briefly recalled in this Section.

4.1 Spectral Kurtosis

Let $x(t)$ be a scalar-valued, zero-mean stationary random process, t being the time, which can be represented in the frequency domain by the Stieltjes integral (Priestley 1981):

$$x(t) = \int_{-\infty}^{\infty} \mathrm{e}^{\mathrm{i}\omega t}\, \mathrm{d}X(\omega) \tag{1}$$

where $X(\omega)$ is a complex-valued random process (as a function of the circular frequency ω), whose increments $\mathrm{d}X(\omega) = X(\omega+\mathrm{d}\omega) - X(\omega)$ are circular-complex random variables (CCRV) (Amblard et al 1996) fulfilling the relationship:

$$\mathrm{E}\left[\mathrm{d}X(\omega)\,\mathrm{d}X^*(\omega')\right] = \begin{cases} S_x(\omega)\,\mathrm{d}\omega & \text{if } \omega=\omega' \\ 0 & \text{otherwise} \end{cases} \tag{2}$$

in which $\mathrm{E}[\cdot]$ is the expectation operator and $S_x(\omega)$ is the PSD of $x(t)$.

The Spectral Kurtosis (SK) of $x(t)$ is defined as (Ottonello & Pagan 1994):

$$K_x(\omega) = \frac{\mathrm{E}\left[\left|\mathrm{d}X(\omega)\right|^4\right]}{\mathrm{E}\left[\left|\mathrm{d}X(\omega)\right|^2\right]^2} - 2 \tag{3}$$

It can be easily shown that, if $\mathrm{d}X(\omega)$ is a Gaussian CCRV, then its SK vanishes. This property is fulfilled, obviously, by Gaussian random processes, but can be extended to the class of the so-called mixing processes (e.g. processes whose multiple-time correlations of any order are absolutely integrable).

Also, it can be demonstrated that if $y(t)$ is a harmonic process with circular frequency $\overline{\omega}$ and uniformly-distributed phase angles, then it results $K_y(\overline{\omega}) = -1$. When a process $z(t)$ is composed by a pure tone $y(t)$ contaminated by a stationary random process $x(t)$, then its SK is given by the relationship (Vrabie et al 2003):

$$K_z(\overline{\omega}) = -\left(\frac{SNR(\overline{\omega})}{1+SNR(\overline{\omega})}\right)^2 \tag{4}$$

where *SNR* is the signal-to-noise ratio. According to Eq. (4), the SK K_z results bounded in [-1, 0].

Finally, it was proved that the presence in the signals of intermittent components with typical return period larger than the length of the time window used for the computation of the spectrogram is reflected by values of SK greater than zero (Antoni 2006).

4.2 Proper Orthogonal Decomposition

Let $\mathbf{x}(t)$ be a vector-valued (N-variate) stationary, zero-mean random process, represented in the frequency domain by a relationship analogous to Eq. (1), in which $\mathbf{X}(\omega)$ is vector-valued as well. According to the Proper Orthogonal Decomposition (POD), the increments $d\mathbf{X}(\omega)$ can be represented by the modal expansion:

$$d\mathbf{X}(\omega) = \sum_{k=1}^{N} \boldsymbol{\theta}_k(\omega) \sqrt{\gamma_k(\omega)}\, dB_k(\omega) \qquad (5)$$

where γ_k and $\boldsymbol{\theta}_k$ are, respectively, the eigenvalues and the eigenvectors of the PSD matrix $\mathbf{S}_\mathbf{x}(\omega)$ of the process $\mathbf{x}(t)$, while $B_k(\omega)$ are uncorrelated Wiener processes whose increments fulfill the relationship:

$$\mathrm{E}\left[dB_k(\omega)\, dB_h^*(\omega) \right] = d\omega \delta_{hk} \qquad (6)$$

δ_{hk} being the Kronecker delta. The eigenvectors $\boldsymbol{\theta}_k(\omega)$ represent, for any frequency value ω, the shape of a coherent component of the process, whose spectral power is given by the corresponding eigenvalue. The case in which an eigenvalue (e.g. γ_1) is much greater than the others at some frequency $\bar{\omega}$ is particularly relevant since it indicates that the process $\mathbf{x}(t)$ is dominated, in the neighborhood of $\bar{\omega}$, by a coherent mode whose amplitude and phase are given by the components of $\boldsymbol{\theta}_1(\bar{\omega})$.

5. DISCUSSION OF THE RESULTS

The color-map reported in Figure 4 shows the log-amplitude of the PSD of the pressure measured by the sensor p_3 (Fig. 1), estimated in a time-window moving along the startup period considered in Figure 2. The abscissa represents the frequency, $n=\omega/2\pi$, normalized by the shaft frequency, n_0=8.29 Hz (500 rpm, nominal). The signature of the impeller rotational speed (n/n_0 = 1) and of the blade-passing frequency (n/n_0 = 5) are clearly visible. Besides these two spectral components (invariant with the time), further narrow-band components appear as soon as the last stage absolute pressure drops below a value about 500 mbar (see Figure 2). As the suction pressure is further reduced, these spectral peaks become more and more focalized, shift and eventually form a pattern symmetrical with respect to n/n_0 =2.5.

Figure 5 shows the time-evolution of the PSD of the acceleration measured by the sensor a_1 (Fig. 1), estimated in a window moving along the time scale adopted in Figure 3. Besides the straight lines corresponding to the shaft rotational speed and its super-harmonics, two straight lines about n/n_0= 6 – 7 can be easily distinguished and, as it is discussed in the following, correspond to the first two mechanical resonances of the pump frame. The harmonic components already observed in the pressure measurements (Fig. 4) are visible here as well, forming a pattern that change as a function of the flow. The presence of a narrow-band harmonic component approaching the second natural frequency form above in maximum flow condition is worth noting since, as it can be expected, this circumstance has a relevant impact on the measured vibration amplitude.

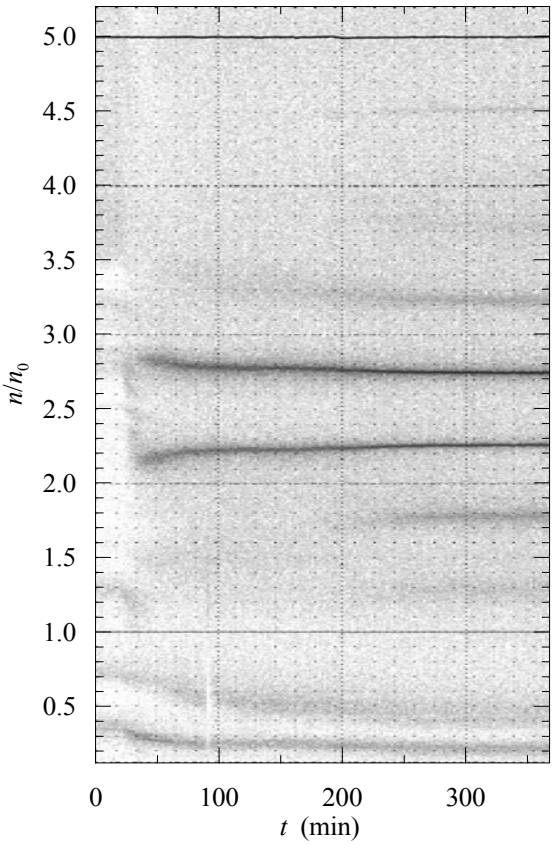

Figure 4: *time evolution of the PSD of the pressure p_3 during the startup operation shown in Figure 2.*

The results of some further analyses carried out on a time window corresponding to the first 100 minute of the time scale in adopted in Figure 3 are here presented and discussed. In that period, the plant was operated in stationary condition at maximum flow. Figure 6 shows the PSD (a) and the SK (b) of the pressure measurements obtained by the sensor p_3. Several peaks can be clearly distinguished either at synchronous (symbol ○) and non-synchronous frequencies (symbol □). The higher peaks of the PSD tend to have SK close to minus 1, indicating the presence of a dominant pure-tone component at that frequency. This result was expected for synchronous frequencies, but is not obvious for the other peaks.

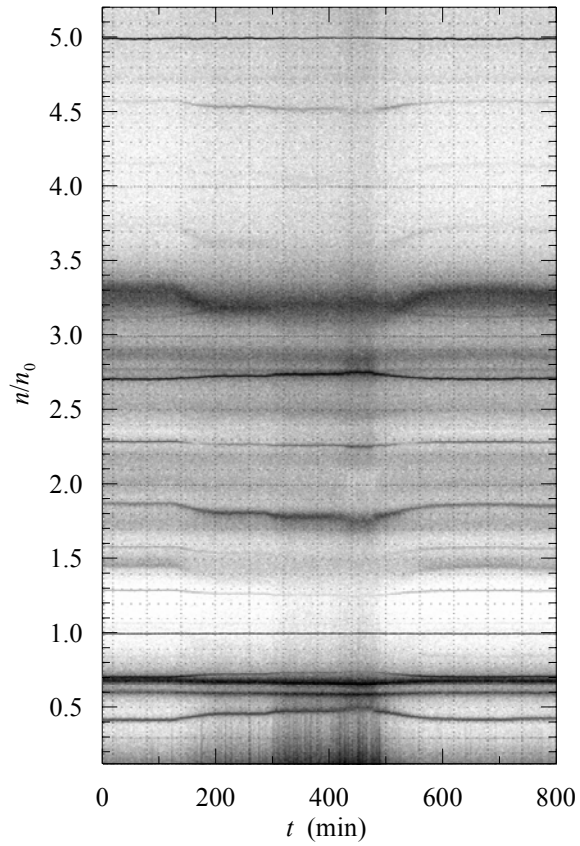

Figure 5: *time evolution of the PSD of the acceleration a_1 during the operation shown in Figure 3.*

Figure 7 is analogous to Figure 6, but is referred to the accelerometer a_1. Also in this case, synchronous and non-synchronous pure-tone components can be distinguished. Most of the peaks correspond to the ones observed in the pressure measurements, however, two peaks clearly visible in the PSD of the acceleration (n/n_0 = 0.60 and 0.69, symbol △) are not present in PSD of the pressure (Fig. 6). These peaks have been interpreted as the trace of the mechanical resonances, since their frequency is not affected by flow variations (Fig. 5). This hypothesis can be reinforced noting that the SK estimated at the above frequencies does not present any negative peak; this circumstance demonstrates that the mentioned peaks in the PSD are not related to pure-tone components and are likely to be associated to resonant amplifications. It is worth noting that the SK is able to detect a pure-tone component at n/n_0 = 0.71, very close to the peak of the second vibration mode.

Figure 8 shows the amplitude of the first POD eigenvector of the 4 acceleration signals calculated at n/n_0=0.60 (a) and n/n_0=0.69 (b). At these frequencies, the components of the first POD eigenvector have constant phase angle, thus the plots in Figure 8 represent the shape of the operational modes vibration. It is worth noting that these results are in agreement with the symmetry of the pump frame.

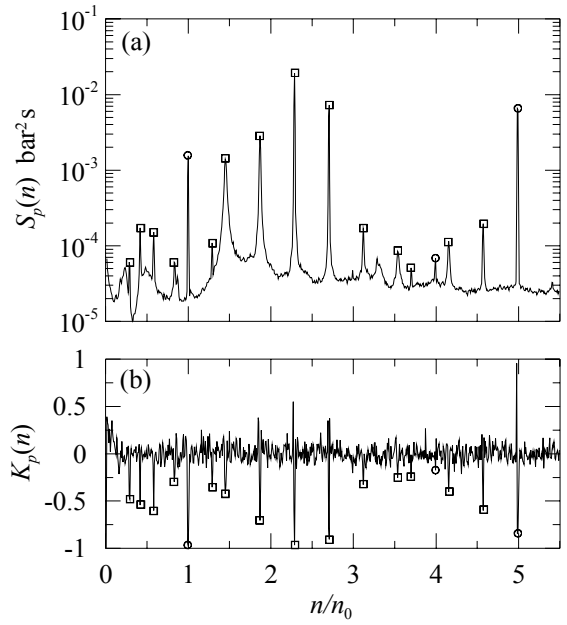

Figure 6: *PSD* (*a*) *and SK* (*b*) *of the pressure p_3. Peaks at synchronous* (○) *and non-synchronous* (□) *frequencies.*

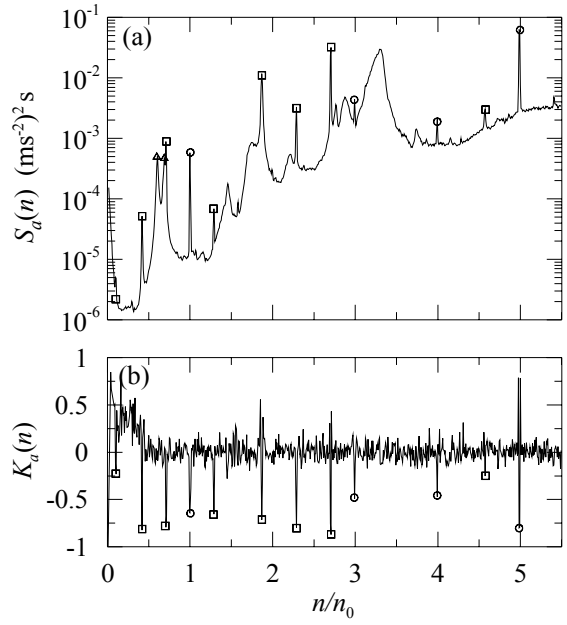

Figure 7: *PSD* (*a*) *and SK* (*b*) *of the acceleration a_1. Peaks at synchronous* (○) *and non-synchronous* (□) *frequencies; resonances* (△).

Figure 9 shows the first POD eigenvector of the pressure signals obtained from the sensors $p_4 - p_7$ and p_9 (sensor p_8 failed) installed on the outer surface of the upper bell mouth. For both the showed eigenvectors, all the components have a common phase angle. Figure 9a is obtained at the frequency of the higher non-synchronous peak in the PSD (n/n_0 = 2.29) and represents a spatially-uniform pressure field; Figure 9b is obtained at the

frequency of the first vibration mode (n/n_0 = 0.60) and represents a pressure field that seems to be determined by the motion of the pump (see Figure 8a for the comparison).

Figure 10 shows the modulus (a) and the real part (b) of the first POD eigenvalue of the pressure signal $p_4 - p_7$ and p_9 estimated at the impeller frequency (n/n_0 = 1.00). The pressure field at this frequency is dominated by a coherent component with spatially-uniform intensity, but rotating with the same speed of the impeller. The real part of the eigenvector shown in Figure 10b can be regarded as a snapshot of the fluctuating part of the pressure field.

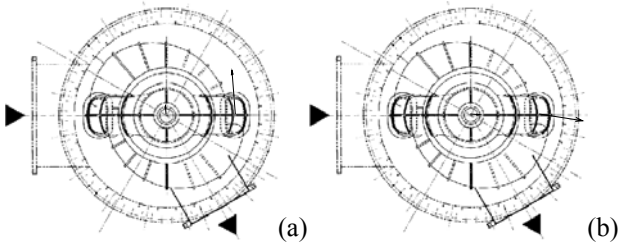

Figure 8: *First POD eigenvector of the acceleration estimated at n/n_0=0.60 (a) and n/n_0=0.69 (b).*

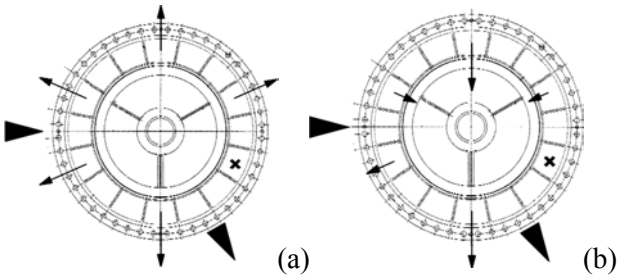

Figure 9: *First POD eigenvector of the pressure estimated at n/n_0=2.29 (a) and n/n_0=0.60 (b).*

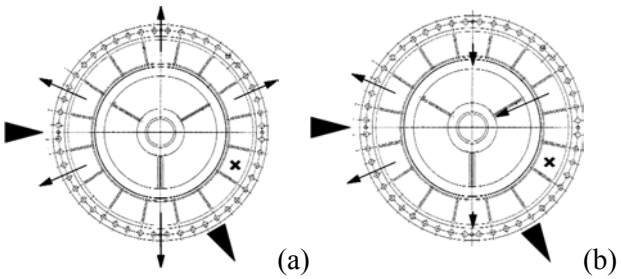

Figure 10: *Modulus (a) and real part (b) of the first POD eigenvector of the pressure estimated at n/n_0=1.00.*

6. CONCLUSION

Pressure and vibration measurements carried out in a BRP demonstrated the existence of a quite complex dynamical behavior triggered by the suction pressure. Several spectral peaks were detected and analyzed by means of the tools provided by the classical spectral analysis, as well as by more specialized techniques such as SK and POD. Two of the recognized non-synchronous pure-tone peaks were clamed as responsible for the large-amplitude vibration observed in some working conditions in which quasi-resonant regimes were recognized.

Although the physical cause producing the mentioned peaks has not been fully understood, it is worth mentioning, that immediately after the reported measurements, the suction bells of some pumps were replaced with new ones having a different design (mainly on their exterior part). The replacement was totally independent of the finding of the analyses described herein and was not aimed at improving the hydrodynamics of the pump, however it happened that most of the spectral peaks here observed disappeared, including the ones responsible for the large-amplitude vibration. At the present stage, the reason for such a modification of the dynamic behavior is not clear and is under investigation.

7. ACKNOWLEDGEMENTS

The authors are indebted with the Owner and O&M companies of the plant for allowing the publication of the results presented herein. The careful technical and logistic work of Mr A. Baghino and Mr A. Silvestri (Fisia Italimpianti) that made the reported experimentation feasible is gratefully acknowledged.

8. REFERENCES

Amblard, P.O. et al, 1996, Statistics for complex random variables and signals – part i: variables, *Signal Processing*, **53**: 1-13.

Antoni, J., 2006, The spectral kurtosis: a useful tool for characterising non-stationary signals. *Mechanical Systems and Signal Processing*, **20**: 282-307.

Holmes, P., Lumley, J.L. and Berkooz, G., 1996. *Turbulence: coherent structures, dynamical systems and symmetry*, Cambridge University Press, UK.

Ottonello, C., Pagan, S., 1994, Modified frequency-domain kurtosis for signal processing, *Electronics Letters*, **30**: 1117-1118.

Priestley, P.J., 1981. *Spectral analysis and time series*. Academic Press, London.

Vrabie, V.D. et al, 2003, Spectral kurtosis: from definition to application, in: IEEE-EURASIP *Workshop on Nonlin. Sign. and Image Proc.,* Grado, Italy 8-11 June 2003.